LARGE SCALE IMAGE COMPLETION VIA CO-MODULATED GENERATIVE ADVERSARIAL NETWORKS

Anonymous authors
Paper under double-blind review

ABSTRACT

Numerous task-specific variants of conditional generative adversarial networks have been developed for image completion. A serious limitation is revealed that all existing algorithms tend to fail when handling large-scale missing regions. To overcome this challenge, we propose a generic new approach that bridges the gap between image-conditional and recent modulated unconditional generative architectures via *co-modulation* of both conditional and stochastic style representations. Due to the lack of good quantitative metrics for image completion, we propose the new *Paired/Unpaired Inception Discriminative Score (P-IDS/U-IDS)*, which robustly reflects the perceptual fidelity of inpainted images compared to real images based on a machine discriminator. Experiments demonstrate superior performance over state-of-the-art methods in free-form image completion and easy generalization to image-to-image translation in terms of both quality and diversity.

1 INTRODUCTION

Generative adversarial networks (GANs) have received a great amount of attention in the past few years. A fundamental problem emerges from the divergence of development between image-conditional and unconditional GANs. Image-conditional GANs have a wide variety of computer vision applications (Isola et al., 2017). While vanilla U-Net-like generators cannot achieve promising performance especially in free-form image completion (Liu et al., 2018; Yu et al., 2019), a multiplicity of task-specific approaches have been proposed to specialize GAN frameworks, mostly focused on hand-engineering multi-stage architectures, specialized operations, and intermediate structures like edges or contours (Altinel et al., 2018; Ding et al., 2018; Iizuka et al., 2017; Jiang et al., 2019; Lahiri et al., 2020; Li et al., 2020; Liu et al., 2018; 2019a; 2020; Nazeri et al., 2019; Ren et al., 2019; Wang et al., 2018; Xie et al., 2019; Xiong et al., 2019; Yan et al., 2018; Yu et al., 2018; 2019; Yu et al., 2019; Zeng et al., 2019; Zhao et al., 2020; Zhou et al., 2020). These branches of works have made significant progress in reducing the generated artifacts like color discrepancy and blurriness. However, a serious challenge is revealed that all existing algorithms tend to fail when handling large-scale missing regions. This is mainly due to their unawareness of the underlying generative capability — one would never learn to complete a large proportion of an object as long as it does not have the capability of generating a completely new one. We argue that the key to overcome this challenge is to *bridge the gap between image-conditional and unconditional generative architectures*.

Recently, the performance of unconditional GANs has been fundamentally advanced, owing to the success of modulation approaches (Chen et al., 2019; Karras et al., 2019a;b) with learned style representations produced by the latent vector. Researchers have been extending modulation approaches to the image-conditional setting, where the style representations are fully determined by an input image (Park et al., 2019; Huang et al., 2018; Liu et al., 2019b); however, the absence of stochasticity makes them hardly generalizable to the settings where limited conditional information is available. This is fatal especially in large scale image completion. Even though some multi-modal unpaired image-to-image translation methods propose to encode the style from another reference image (Huang et al., 2018; Liu et al., 2019b), this unreasonably assumes that the style representations are completely independent of the conditional input and hence compromises the paired consistency.

Therefore, we propose the *co-modulated generative adversarial networks*, a generic approach that leverages the generative capability from the unconditional modulated architectures and embeds both *conditional* and *stochastic* style representations via *co-modulation*. Co-modulated GANs are able to

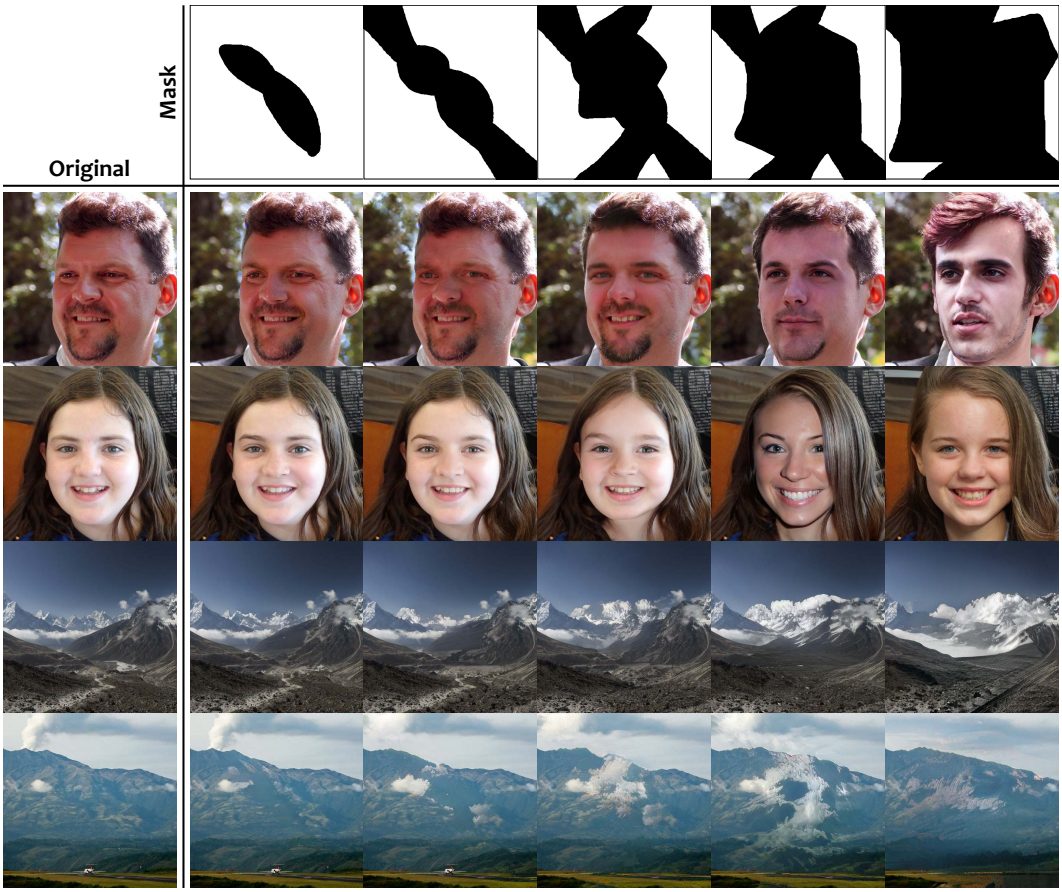

Figure 1: **Our image completion results w.r.t. different masks.** Our method successfully bridges differently conditioned situations, from small-scale inpainting to large-scale completion (left to right). The original images are sampled at 512×512 resolution from the FFHQ dataset (Karras et al., 2019a) within a 10k validation split (top two examples) and the Places2 validation set (Zhou et al., 2017) (bottom two examples). We refer the readers to the appendix for extensive qualitative examples.

generate stochastically consistent contents and generalize well to not only small-scale inpainting but also extremely large-scale image completion, supporting both regular and irregular masks even when there is little conditional information. See Fig. 1 for qualitative examples. Due to the effectiveness of co-modulation, we do not encounter any problem suffered in the image completion literature (Liu et al., 2018; Yu et al., 2019) hence successfully bridge the long-existing divergence.

Another major barrier in the image completion literature is due to the lack of good quantitative metrics. The vast majority of works in this literature seek to improve their performance in terms of similarity-based metrics that heavily prefer blurry results, e.g., L_1, L_2, PSNR, and SSIM, while many state that *there is yet no good quantitative metric for image completion* (Liu et al., 2018; Yu et al., 2018; 2019). The only gold standard in this literature is the user study, which conducts real vs. fake test once given a pair of images to the users. However, the user study is inaccurate and costly, while strongly depending on the particular setting, and hence deviates from the reproducibility. Inspired by the user study, we propose the new *Paired/Unpaired Inception Discriminative Score (P-IDS/U-IDS)*. Besides its intuitiveness and scalability, we demonstrate that P-IDS/U-IDS is robust to sampling size, effective of capturing subtle differences, and correlates well to human preferences.

Our contributions are summarized as follows:

- We propose the *co-modulated GANs*, a generic approach that bridges the gap between image-conditional and recent modulated unconditional generative architectures.
- We propose the new *P-IDS/U-IDS* for robustly assessing the perceptual fidelity for GANs.

- Experiments demonstrate superior performance in free-form image completion and easy generalization to image-to-image translation in terms of both quality and diversity.

2 Related Work

Image-Conditional GANs. Image-conditional GANs can be applied to a variety of image-to-image translation tasks (Isola et al., 2017). The unpaired setting is also investigated when paired training data is not available (Choi et al., 2018; Huang et al., 2018; Kim et al., 2019; Liu et al., 2017; Yi et al., 2017; Zhu et al., 2017a). Recent works exploit normalization layers with learned style representations embedded from the conditional input or another reference image to enhance the output fidelity (Huang et al., 2018; Kim et al., 2019; Liu et al., 2019b; Park et al., 2019). They can be regarded as a set of conditional modulation approaches, but still lack stochastic generative capability and hence poorly generalize when limited conditional information is available. Isola et al. (2017) initially find that the generator tends to ignore the noise input although they try to feed it, in contrast to unconditional or class-conditional GANs. A branch of works aims to enforce the intra-conditioning diversity using VAE-based latent sampling strategies (Zhu et al., 2017b) or imposing distance-based loss terms (Huang et al., 2018; Mao et al., 2019; Qin et al., 2018). Wang et al. (2019b) also propose to decompose the convolution kernels into stochastic basis. However, the enforcement of diversity conversely results in the deterioration of image quality. Our co-modulation approach not only learns the stochasticity inherently but also makes the trade-off easily controllable.

Image Completion. Image completion, also referred to as image inpainting when incapable of completing large-scale missing regions, has received a significant amount of attention. It is a constrained image-to-image translation problem but exposes more serious challenges. Traditional methods (Ballester et al., 2001; Barnes et al., 2009; Darabi et al., 2012; Efros & Freeman, 2001; Efros & Leung, 1999) utilize only low-level features and fail to generate semantically consistent contents. Then, (Köhler et al., 2014; Ren et al., 2015; Xie et al., 2012) adopt deep neural networks for image completion; (Pathak et al., 2016) first exploits conditional GANs. Numerous follow-up works focus on the semantic context and texture, edges and contours, or hand-engineered architectures (Altinel et al., 2018; Ding et al., 2018; Iizuka et al., 2017; Jiang et al., 2019; Jo & Park, 2019; Lahiri et al., 2017; Liu et al., 2019a; Nazeri et al., 2019; Ren et al., 2019; Sagong et al., 2019; Wang et al., 2018; Xie et al., 2019; Xiong et al., 2019; Yan et al., 2018; Yang et al., 2017; 2019a; Yu et al., 2018; Yu et al., 2019; Zeng et al., 2019; Lahiri et al., 2020; Zhao et al., 2020; Li et al., 2020; Zhou et al., 2020), among which (Liu et al., 2018; Yu et al., 2019) introduce partial convolution and gated convolution to address free-form image completion. The lack of stochasticity is also observed in image completion (Cai & Wei, 2019; Ma et al., 2019; Zheng et al., 2019). Other works address the so-called outpainting subtasks (Sabini & Rusak, 2018; Wang et al., 2019a; Yang et al., 2019b). To our knowledge, none of these methods produce promising results in the presence of free-form large-scale missing regions.

Evaluation Metrics. Great research interest has been drawn on the evaluation of GANs (DeVries et al., 2019; Gurumurthy et al., 2017; Sajjadi et al., 2018; Snell et al., 2017; Xiang & Li, 2017). Inception Score (IS) (Salimans et al., 2016), and some other metrics like FCN-Score (Isola et al., 2017), are specialized to the pre-trained task thus cannot generalize. While FID (Heusel et al., 2017) is generally acceptable, few promising metrics for image completion exist. Previous works heavily rely on similarity-based metrics such as L_1, L_2, PSNR, and SSIM, which fail to capture stochastic regions and are ill-fitted for GANs. Our proposed metric is also related to the classifier-based tests (Blau & Michaeli, 2018; Lopez-Paz & Oquab, 2016). However, previous classifier-based metrics require separate sets for training and testing the classifier, making them sensitive to the underlying generalizability of the trained classifier. We formulate the discriminability as a simple scalable metric for both the paired and unpaired versions without relying on the generalizability.

3 Co-Modulated Generative Adversarial Networks

Image-conditional GANs address the problem of translating an image-form conditional input $\boldsymbol{y}$ to an output image $\boldsymbol{x}$ (Isola et al., 2017). We assume for the setting where paired correspondence between input conditions and output images is available in the training data. The generator takes as input an image $\boldsymbol{y}$ along with the latent vector $\boldsymbol{z}$ and produces the output $\boldsymbol{x}$; the discriminator takes as input a pair of $(\boldsymbol{x}, \boldsymbol{y})$ and seeks to distinguish fake generated pairs from the real distribution. Image

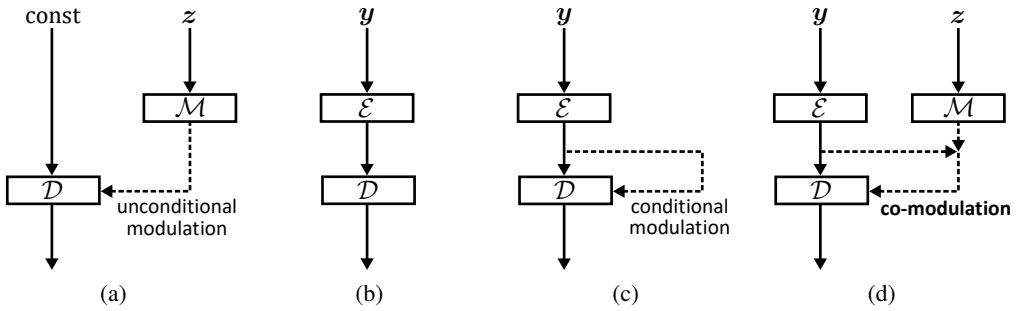

Figure 2: **Illustration from modulation to co-modulation:** (a) unconditional modulated generator; (b) vanilla image-conditional generator; (c) conditional modulated generator; and (d) *co-modulated* generator. $\boldsymbol{y}, \boldsymbol{z}$ represent the conditional input and the latent vector respectively; $\mathcal{E}, \mathcal{D}, \mathcal{M}$ represent the conditional encoder, the generative decoder, and the mapping network, respectively.

completion can be regarded as a constrained image-conditional generation problem where known pixels are restricted to be unchanged. In contrast to the extensive literature on specialized image completion frameworks, we introduce a generic approach that bridges between image-conditional GANs and recent success of unconditional modulated architectures.

3.1 Revisiting Modulation Approaches

Modulation approaches emerge from the style transfer literature (Dumoulin et al., 2016; Huang & Belongie, 2017) and are well exploited in state-of-the-art unconditional or class-conditional GANs. They generally apply scalar denormalization factors (e.g., bias and scaling) to the normalized feature maps, while the learned denormalization factors are conditioned on the side information such as class label (Odena et al., 2018) or the latent vector (Chen et al., 2019). Typical normalization layers used in the modulation blocks include batch normalization (Chen et al., 2019; Odena et al., 2018), adaptive instance normalization (Huang & Belongie, 2017; Karras et al., 2019a), and weight demodulation (Karras et al., 2019b) referred to the weight normalization (Salimans & Kingma, 2016).

Here we take StyleGAN2 (Karras et al., 2019b) as an example to show how intermediate activations are modulated as a function of the latent vector. As illustrated in Fig. 2(a), the decoder $\mathcal{D}$ simply originates from a learned constant, while the latent vector $\boldsymbol{z}$ is passed through a multi-layer fully connected mapping network $\mathcal{M}$. The mapped latent vector linearly generates a style vector $\boldsymbol{s}$ for each subsequent modulation via a learned affine transformation $\mathcal{A}$ (i.e., a dense layer without activation):

$$\boldsymbol{s} = \mathcal{A}(\mathcal{M}(\boldsymbol{z})). \tag{1}$$

Consider a vanilla convolutional layer with kernel weights w_{ijk}, where i, j, k enumerate the input channels, the output channels, and the spatial footprint of the convolution, respectively. Given the style vector $\boldsymbol{s}$, the input feature maps are first channel-wise multiplied by $\boldsymbol{s}$, passed through the convolution, and finally channel-wise multiplied by $\boldsymbol{s}'$ where $s'_j = \sqrt{1/\sum_{i,k}(s_i w_{ijk})^2}$ acting as the weight demodulation step that normalizes the feature maps into statistically unit variance.

While modulation approaches have significantly improved the performance of unconditional or class-conditional generators, we wonder whether they could similarly work for image-conditional generators. An intuitive extension to the vanilla image-conditional generator (Fig. 2(b)) would be the conditional modulated generator (see Fig. 2(c)), where the modulation is conditioned on the learned flattened features from the image encoder $\mathcal{E}$. Similar structures also exist in the well-conditioned image-to-image translation tasks (Huang et al., 2018; Liu et al., 2019b; Park et al., 2019). In this case, the style vector can be rewritten as

$$\boldsymbol{s} = \mathcal{A}(\mathcal{E}(\boldsymbol{y})). \tag{2}$$

However, a significant drawback of the conditional modulation approach would be the lack of stochastic generative capability. This problem emerges more apparently in respect of *large scale* image completion. In most cases, the outputs should be *weakly conditioned*, i.e., they are *not*

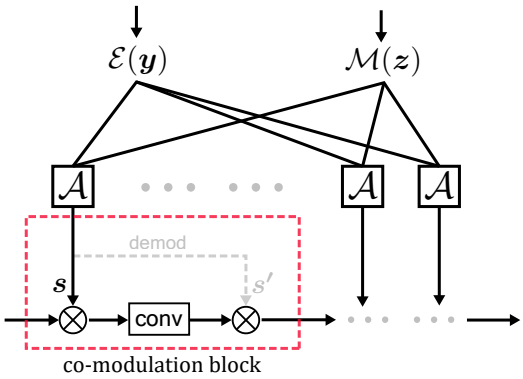

Figure 3: **Co-modulated generative architectures.** Encoded style representations from both the conditional input $\boldsymbol{y}$ and the latent vector $\boldsymbol{z}$ jointly co-modulate a convolutional layer in the generative decoder, with the purpose of promoting stochasticity without loss of consistency.

sufficiently determined by the conditional input. As a result, it not only cannot produce diverse outputs but also poorly generalizes to the settings where limited conditional information is available.

3.2 Co-Modulation

To overcome this challenge, we propose *co-modulation*, a generic new approach that easily adapts the generative capability from the unconditional modulated generators to the image-conditional generators. We rewrite the *co-modulated* style vector as (see Fig. 2(d)):

$$\boldsymbol{s} = \mathcal{A}(\mathcal{E}(\boldsymbol{y}), \mathcal{M}(\boldsymbol{z})), \tag{3}$$

i.e., a joint affine transformation conditioning on both style representations. Generally, the style vector can be a non-linear learned mapping from both inputs, but here we simply assume that they can be linearly correlated in the style space and already observe considerable improvements. The linear correlation facilitates *the inherent stochasticity* as will see in §5.1 that co-modulated GANs can easily trade-off between quality and intra-conditioning diversity without imposing any external losses, and moreover, co-modulation contributes to not only stochasticity but also visual quality especially at large-scale missing regions. Fig. 3 provides an in-depth illustration of the proposed co-modulated generative architectures. Each *co-modulation block* conditionally and stochastically co-modulates a convolutional layer in the generative decoder, using weight demodulation as the normalization layer as revisited in §3.1. See Appendix A for more implementation details. Co-modulated GANs are encouraged to be trained with regular discriminator losses, while not requiring any direct guidance like the L_1 term (Isola et al., 2017), to fully exploit their stochastic generative capability.

4 Paired/Unpaired Inception Discriminative Score

Our proposed *Paired/Unpaired Inception Discriminative Score (P-IDS/U-IDS)* aims to reliably measure the linear separability in a pre-trained feature space, inspired by the "human discriminators" in the user study. Let $\mathcal{I}(\cdot)$ be the pre-trained Inception v3 model that maps the input image to the output features of 2048 dimensions. We sample the same number of real images and their correspondingly generated fake images (drawn from the joint distribution $(\boldsymbol{x}, \boldsymbol{x}') \in \boldsymbol{X}$, where $\boldsymbol{x}$ corresponds to the real image and $\boldsymbol{x}'$ corresponds to the fake image), from which the features are extracted and then fitted by a linear SVM. The linear SVM reflects the linear separability in the feature space and is known to be numerically stable in training. Let $f(\cdot)$ be the (linear) decision function of the SVM, where $f(\mathcal{I}(\boldsymbol{x})) > 0$ if and only if $\boldsymbol{x}$ is considered real. The P-IDS is given by

$$\textbf{P-IDS}(\boldsymbol{X}) = \Pr_{(\boldsymbol{x},\boldsymbol{x}') \in \boldsymbol{X}} \{f(\mathcal{I}(\boldsymbol{x}')) > f(\mathcal{I}(\boldsymbol{x}))\}, \tag{4}$$

i.e., the probability that a fake sample is considered more realistic than the corresponding real sample.

We also provide an *unpaired* alternative that could generalize to the settings where no paired information is available. We similarly sample the same number of real images (drawn from distribution X)

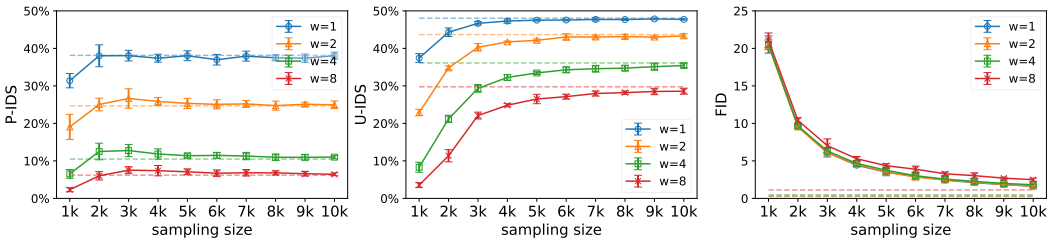

Figure 4: **Robustness to sampling size.** Dashed convergence lines are measured using 50k samples. P-IDS/U-IDS converges fast; FID fails to converge within 10k samples. Results are averaged over 5 runs; error bars indicate standard deviations.

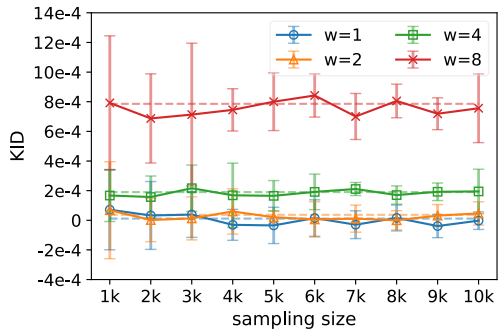

Figure 5: **Kernel Inception Distance (KID) still suffers from large variance.** Although it achieves unbiased estimates, the huge variance even makes them often negative and hardly distinguishable. Results are averaged over 5 runs; error bars indicate standard deviations.

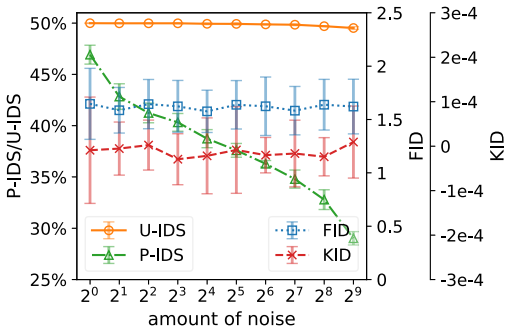

Figure 6: **Effectiveness of capturing subtle differences.** All metrics are measured using 10k samples. P-IDS effectively reflects the amount of noise; FID and KID fail to respond within 2^9 noisy pixels. Results are averaged over 5 runs; error bars indicate standard deviations.

and fake images (drawn from distribution X') and fit the linear SVM $f(\cdot)$. We directly calculate the misclassification rate instead:

$$\textbf{U-IDS}(X, X') = \frac{1}{2} \Pr_{\boldsymbol{x} \in X} \{f(\mathcal{I}(\boldsymbol{x})) < 0\} + \frac{1}{2} \Pr_{\boldsymbol{x}' \in X'} \{f(\mathcal{I}(\boldsymbol{x}')) > 0\}. \tag{5}$$

In addition to the super intuitiveness of P-IDS/U-IDS, we would like to emphasize three of their major advantages over FID: the robustness to sampling size, the effectiveness of capturing subtle differences, and the good correlation to human preferences.

Robustness to Sampling Size. We test the response of P-IDS, U-IDS, FID, and KID to four manipulation strategies: masking the image (to zeros) with a random square of width $w = 1, 2, 4, 8$, respectively. Images are sampled from the FFHQ dataset (Karras et al., 2019a) at 512×512 resolution. The reference distribution for calculating FID is measured using 50k samples. As plotted in Fig. 4, both P-IDS and U-IDS converge fast within a small number of samples and successfully distinguish the manipulation strategies; FID fails to converge within 10k samples, while the highest convergence line (1.13 when $w = 8$, measured using 50k samples) is even below the lowest FID at 10k samples (1.63 when $w = 1$). Although KID addresses the "biased" problem of FID (Bińkowski et al., 2018), we find that the estimates are still subject to huge variance like FID especially when the two distributions are close. KID requires a fixed block size (Bińkowski et al., 2018) to achieve unbiased estimates; even with a block size of 1000 that minimizes its variance, the estimates are still hardly distinguishable especially between $w = 1$ and $w = 2$ as plotted in Fig. 5.

Effectiveness of Capturing Subtle Differences. Capturing subtle differences is particularly important in image completion, since the difference between inpainted and real images only exists in a partial region. We construct subtle image manipulation strategies by masking n random pixels which are then nearest-point interpolated by the neighboring pixels, using the same environment as the last experiment. As plotted in Fig. 6, P-IDS successfully distinguishes the number of manipulated pixels,

Table 1: **Quantitative results for large scale image completion.** Our method is compared against DeepFillv2 (Yu et al., 2019) and RFR (Li et al., 2020). Results are averaged over 5 runs.

Method	FFHQ			Places2		
	P-IDS (%)	U-IDS (%)	FID	P-IDS (%)	U-IDS (%)	FID
RFR (official)	0.0 ± 0.0	0.0 ± 0.0	48.7 ± 0.5	0.3 ± 0.0	4.6 ± 0.0	49.6 ± 0.2
DeepFillv2 (official)	0.0 ± 0.0	0.1 ± 0.0	83.5 ± 0.6	0.8 ± 0.0	8.4 ± 0.0	30.6 ± 0.2
DeepFillv2 (retrained)	0.9 ± 0.1	8.6 ± 0.2	17.4 ± 0.4	1.4 ± 0.0	11.4 ± 0.0	22.1 ± 0.1
Ours	$\mathbf{16.6 \pm 0.3}$	$\mathbf{29.4 \pm 0.3}$	$\mathbf{3.7 \pm 0.0}$	$\mathbf{13.3 \pm 0.1}$	$\mathbf{27.4 \pm 0.1}$	$\mathbf{7.9 \pm 0.0}$

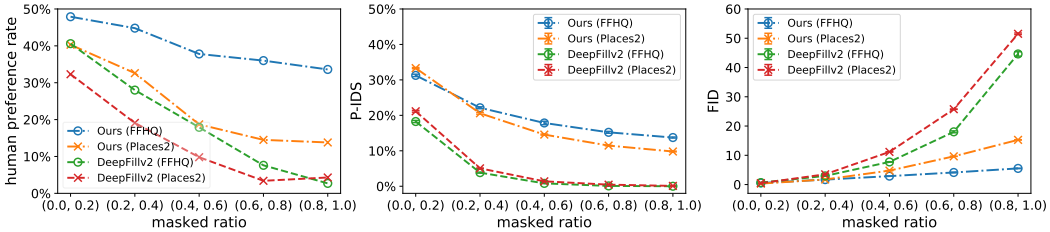

Figure 7: **User study results, P-IDS and FID plots** of DeepFillv2 (retrained) and ours w.r.t. different masked ratios. P-IDS and FID are averaged over 5 runs; error bars indicate standard deviations.

while FID and KID fail to respond within 2^9 noisy pixels. We note that U-IDS is still more robust in this case since the central tendency of FID and KID is significantly dominated by the variance.

Correlation to Human Preferences. P-IDS imitates the "human discriminators" and is expected to correlate well with human preferences. While it seems clear in Fig. 7, we quantitatively measure the correlation using these data points (20 in total): the correlation coefficient is 0.870 between P-IDS and human preference rate, significantly better than -0.765 of FID. Table 3 further provides a case analysis where our P-IDS/U-IDS coincides with clear human preferences as opposed to FID.

Computational Analysis. The time complexity of training a linear SVM is between $O(n^2)$ and $O(n^3)$ (Bottou & Lin, 2007), compared to $O(nd^2 + d^3)$ of FID (Heusel et al., 2017) and $O(n^2 d)$ of KID (Bińkowski et al., 2018), where n is the sampling size and d is the dimension of feature space. In practice, P-IDS/U-IDS incurs mild computational overhead in addition to the feature extraction process. For example, with 10k samples, extracting the Inception features on an NVIDIA P100 GPU takes 221s, and fitting the SVM (which only uses CPU) takes an extra of 88s; with 50k samples, the feature extraction process and the SVM take 1080s and 886s respectively.

5 Experiments

5.1 Image Completion

We conduct image completion experiments at 512×512 resolution on the FFHQ dataset (Karras et al., 2019a) and the Places2 dataset (Zhou et al., 2017). Implementation details are provided in Appendix A. FFHQ is augmented with horizontal flips; Places2 is central cropped or padded. The sampling strategy of free-form masks for training and evaluating is specified in the appendix. We preserve 10k out of 70k images from the FFHQ dataset for validation. Places2 has its own validation set of 36.5k images and a large training set of 8M images. We train our model for 25M images on FFHQ and 50M images on Places2. Our model is compared against RFR (Li et al., 2020) and DeepFillv2 (Yu et al., 2019), the state-of-the-art algorithms for free-form image completion, using both their official pre-trained models and our retrained version of DeepFillv2 (using the official code, our datasets, and our sampling strategy) at 1M iterations (i.e., 32M images). We sample the output once per validation image for all the metrics (P-IDS, U-IDS, and FID). The overall results are summarized in Table 1. Fig. 7 plots the user study results, P-IDS, and FID of DeepFillv2 (retrained) and ours w.r.t. different masked ratios. See Fig. 8 for a qualitative comparison. All these results demonstrate our superior performance. More qualitative examples, numerical user study results and complete tables w.r.t. the masked ratio, and details of the user study are provided in the appendix.

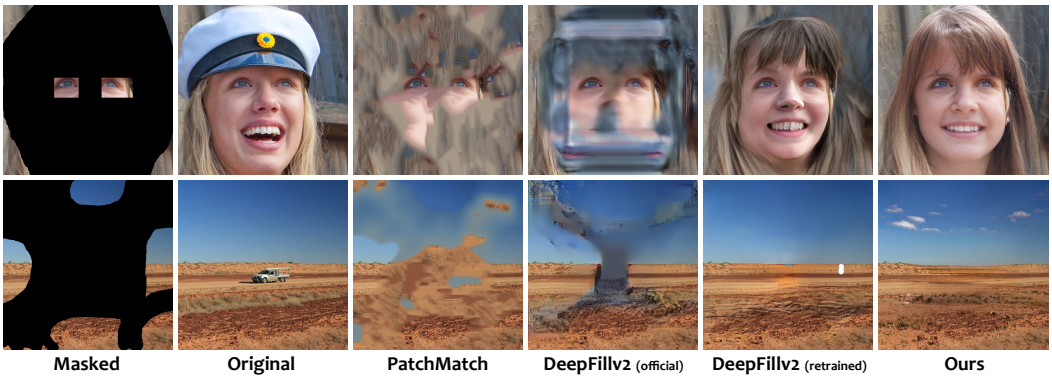

Figure 8: **Qualitative examples of state-of-the-art methods on large scale image completion:** PatchMatch (Barnes et al., 2009), DeepFillv2 (Yu et al., 2019), and ours. The original images are sampled at 512×512 resolution from the FFHQ dataset (Karras et al., 2019a) within a 10k validation split (top) and the Places2 validation set (Zhou et al., 2017) (bottom). We refer the readers to the appendix for extensive qualitative examples.

The Inherent Stochasticity. Co-modulated GANs are inherently stochastic, i.e., they naturally learn to utilize the stochastic style representations without imposing any external losses, and they are able to produce diverse results even when both the input image and the input mask are fixed. Furthermore, by tuning the truncation ψ (Karras et al., 2019b; Kynkäänniemi et al., 2019) that explicitly amplifies the stochastic branch by ψ times, co-modulated GANs can easily trade-off between quality and diversity (see Fig. 9).

Ablation Study. Co-modulation promotes not only stochasticity but also image quality. We compare vanilla, conditional modulated, and co-modulated GANs as illustrated in Figs. 2(b) to 2(d). Experiments are run on the FFHQ dataset with the same setting as § 5.1. While the vanilla version completely fails, our co-modulation approach dominates the conditional modulated version and especially when the masked ratio becomes large (see Fig. 11). We refer the readers to the appendix for the complete results (Table 6). Qualitatively, we often observe some unusual artifacts of the conditional modulated one in the large missing regions (see Fig. 10), which we hypothesize is due to the lack of stochastic generative capability.

5.2 Image-to-Image Translation

Edges to Photos. Co-modulated GANs are generic image-conditional models that can be easily adopted to image-to-image translation tasks. We follow the common setting (DeVries et al., 2019; Wang et al., 2019b) on the edges to photos datasets (Isola et al., 2017) at 256×256 resolution, where

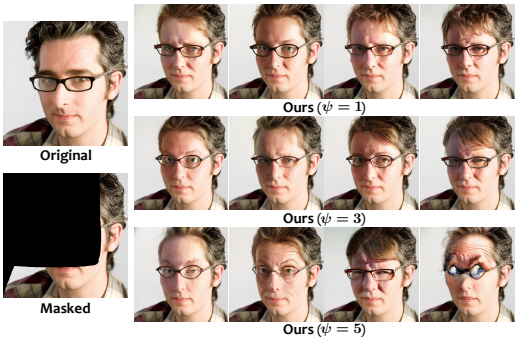

Figure 9: **The inherent stochasticity.** Co-modulated GANs can easily trade-off between quality and diversity by tuning the truncation ψ.

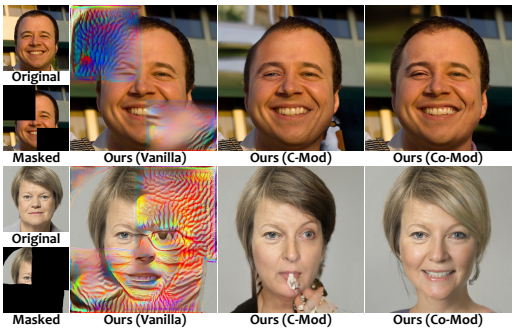

Figure 10: **Qualitative ablation study** among Vanilla, conditional modulation (C-Mod), and our co-modulation (Co-Mod) as in Figs. 2(b) to 2(d).

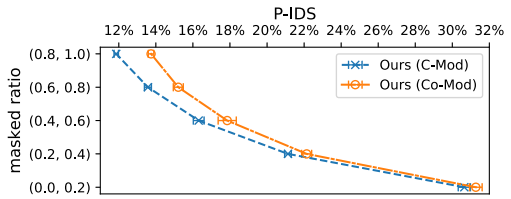

Figure 11: **Co-modulation dominates conditional modulation (C-Mod)** at all masked ratios, especially when the masked ratio becomes large.

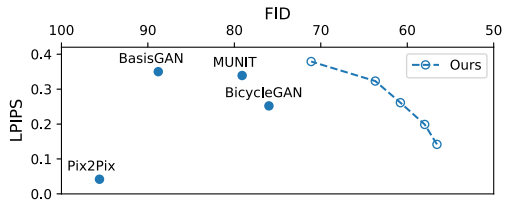

Figure 12: **Trade-off curve** of our method between quality (FID) and diversity (LPIPS) on the Edges2Handbags dataset.

Table 2: Image-to-image translation results on the **edges to photos** (Isola et al., 2017) datasets.

Method	Edges2Shoes		Edges2Handbags	
	FID	LPIPS	FID	LPIPS
Pix2Pix (Isola et al., 2017)	74.2	0.040	95.6	0.042
BicycleGAN (Zhu et al., 2017b)	47.3	0.191	76.0	0.252
MUNIT (Huang et al., 2018)	56.2	0.229	79.1	0.339
BasisGAN (Wang et al., 2019b)	64.2	**0.242**	88.8	0.350
Ours	**38.5**	0.036	**56.9**	0.143
Ours ($\psi = 3$)	**38.5**	0.038	71.1	**0.379**

FID samples once per validation image (200 in total) and the training set is used as the reference distribution; LPIPS measures the intra-conditioning diversity for which we sample 2k pairs. As summarized in Table 2, our approach easily achieves superior fidelity (FID) over state-of-the-art methods (Huang et al., 2018; Isola et al., 2017; Wang et al., 2019b; Zhu et al., 2017b) despite the fact that MUNIT assumes for the different unpaired setting (Huang et al., 2018), and also superior diversity on the Edges2Handbags dataset by simply tuning the truncation ψ as well as in the trade-off view (see Fig. 12). Our model does not learn to produce diverse outputs on the Edges2Shoes dataset despite its high fidelity, which we hypothesize is due to the learned strong correspondence between the input edge map and the color information extracted from the limited training set.

Labels to Photos (COCO-Stuff). We further experiment on the COCO-Stuff dataset (Caesar et al., 2018) at 256×256 resolution following the experimental setting of SPADE (Caesar et al., 2018). The real images are resized to a short edge of 256 and then random cropped. The input label map has 182 classes; an embedding layer is used before feeding it into the network. We sample the output once per validation image (5k in total) for all the evaluation metrics. Table 3 shows that our method matches the FID of SPADE but significantly outperforms its P-IDS and U-IDS, without any direct supervision like the perceptual loss used in SPADE. We further conduct a user study between SPADE and ours. The user study indicates consistent human preference of ours over SPADE in accordance with our proposed P-IDS/U-IDS. Qualitative results and the user study details are provided in the appendix.

Table 3: Image-to-image translation results on the **COCO-Stuff** dataset (labels to photos).

Method	User study (SPADE vs. ours)	P-IDS (%)	U-IDS (%)	FID
SPADE (Park et al., 2019)	41.0%	1.1	5.3	22.6
Ours	**59.0%**	**4.5**	**11.3**	**22.5**

6 Conclusion

We propose the *co-modulated generative adversarial networks*, a generic approach that bridges the gap between conditional and unconditional modulated generative architectures, significantly improves free-form large scale image completion, and easily generalizes to image-to-image translation. We also propose the intuitive new metric — P-IDS/U-IDS — for robustly assessing the perceptual fidelity for GANs. We expect our approach to be a fundamental solution to the image completion literature and contribute as reliable quantitative benchmarks.

REFERENCES

Fazil Altinel, Mete Ozay, and Takayuki Okatani. Deep structured energy-based image inpainting. In *2018 24th International Conference on Pattern Recognition (ICPR)*, pp. 423–428. IEEE, 2018.

Coloma Ballester, Marcelo Bertalmio, Vicent Caselles, Guillermo Sapiro, and Joan Verdera. Filling-in by joint interpolation of vector fields and gray levels. *IEEE transactions on image processing*, 10(8):1200–1211, 2001.

Connelly Barnes, Eli Shechtman, Adam Finkelstein, and Dan B Goldman. Patchmatch: A randomized correspondence algorithm for structural image editing. In *ACM Transactions on Graphics (ToG)*, pp. 24. ACM, 2009.

Mikołaj Bińkowski, Dougal J Sutherland, Michael Arbel, and Arthur Gretton. Demystifying mmd gans. *arXiv preprint arXiv:1801.01401*, 2018.

Yochai Blau and Tomer Michaeli. The perception-distortion tradeoff. In *Proceedings of the IEEE Conference on Computer Vision and Pattern Recognition*, pp. 6228–6237, 2018.

Léon Bottou and Chih-Jen Lin. Support vector machine solvers. *Large scale kernel machines*, 3(1):301–320, 2007.

Holger Caesar, Jasper Uijlings, and Vittorio Ferrari. Coco-stuff: Thing and stuff classes in context. In *Proceedings of the IEEE Conference on Computer Vision and Pattern Recognition*, pp. 1209–1218, 2018.

Weiwei Cai and Zhanguo Wei. Diversity-generated image inpainting with style extraction. *arXiv preprint arXiv:1912.01834*, 2019.

Ting Chen, Mario Lucic, Neil Houlsby, and Sylvain Gelly. On self modulation for generative adversarial networks. In *International Conference on Learning Representations*, 2019. URL `https://openreview.net/forum?id=Hkl5aoR5tm`.

Yunjey Choi, Minje Choi, Munyoung Kim, Jung-Woo Ha, Sunghun Kim, and Jaegul Choo. Stargan: Unified generative adversarial networks for multi-domain image-to-image translation. In *Proceedings of the IEEE conference on computer vision and pattern recognition*, pp. 8789–8797, 2018.

Soheil Darabi, Eli Shechtman, Connelly Barnes, Dan B Goldman, and Pradeep Sen. Image melding: Combining inconsistent images using patch-based synthesis. *ACM Trans. Graph.*, 31(4):82–1, 2012.

Terrance DeVries, Adriana Romero, Luis Pineda, Graham W Taylor, and Michal Drozdzal. On the evaluation of conditional gans. *arXiv preprint arXiv:1907.08175*, 2019.

Ding Ding, Sundaresh Ram, and Jeffrey J Rodríguez. Image inpainting using nonlocal texture matching and nonlinear filtering. *IEEE Transactions on Image Processing*, 28(4):1705–1719, 2018.

Vincent Dumoulin, Jonathon Shlens, and Manjunath Kudlur. A learned representation for artistic style. *arXiv preprint arXiv:1610.07629*, 2016.

Alexei A Efros and William T Freeman. Image quilting for texture synthesis and transfer. In *Proceedings of the 28th annual conference on Computer graphics and interactive techniques*, pp. 341–346. ACM, 2001.

Alexei A Efros and Thomas K Leung. Texture synthesis by non-parametric sampling. In *Proceedings of the seventh IEEE international conference on computer vision*, volume 2, pp. 1033–1038. IEEE, 1999.

Ian Goodfellow, Jean Pouget-Abadie, Mehdi Mirza, Bing Xu, David Warde-Farley, Sherjil Ozair, Aaron Courville, and Yoshua Bengio. Generative adversarial nets. In *Advances in neural information processing systems*, pp. 2672–2680, 2014.

Swaminathan Gurumurthy, Ravi Kiran Sarvadevabhatla, and R Venkatesh Babu. Deligan: Generative adversarial networks for diverse and limited data. In *Proceedings of the IEEE conference on computer vision and pattern recognition*, pp. 166–174, 2017.

Martin Heusel, Hubert Ramsauer, Thomas Unterthiner, Bernhard Nessler, and Sepp Hochreiter. Gans trained by a two time-scale update rule converge to a local nash equilibrium. In *Advances in neural information processing systems*, pp. 6626–6637, 2017.

Xun Huang and Serge Belongie. Arbitrary style transfer in real-time with adaptive instance normalization. In *Proceedings of the IEEE International Conference on Computer Vision*, pp. 1501–1510, 2017.

Xun Huang, Ming-Yu Liu, Serge Belongie, and Jan Kautz. Multimodal unsupervised image-to-image translation. In *Proceedings of the European Conference on Computer Vision (ECCV)*, pp. 172–189, 2018.

Satoshi Iizuka, Edgar Simo-Serra, and Hiroshi Ishikawa. Globally and locally consistent image completion. *ACM Transactions on Graphics (ToG)*, 36(4):107, 2017.

Phillip Isola, Jun-Yan Zhu, Tinghui Zhou, and Alexei A Efros. Image-to-image translation with conditional adversarial networks. In *Proceedings of the IEEE conference on computer vision and pattern recognition*, pp. 1125–1134, 2017.

Jianmin Jiang, Hossam M Kasem, and Kwok-Wai Hung. Robust image completion via deep feature transformations. *IEEE Access*, 7:113916–113930, 2019.

Youngjoo Jo and Jongyoul Park. Sc-fegan: Face editing generative adversarial network with user's sketch and color. *arXiv preprint arXiv:1902.06838*, 2019.

Tero Karras, Samuli Laine, and Timo Aila. A style-based generator architecture for generative adversarial networks. In *Proceedings of the IEEE Conference on Computer Vision and Pattern Recognition*, pp. 4401–4410, 2019a.

Tero Karras, Samuli Laine, Miika Aittala, Janne Hellsten, Jaakko Lehtinen, and Timo Aila. Analyzing and improving the image quality of stylegan. *arXiv preprint arXiv:1912.04958*, 2019b.

Junho Kim, Minjae Kim, Hyeonwoo Kang, and Kwanghee Lee. U-gat-it: unsupervised generative attentional networks with adaptive layer-instance normalization for image-to-image translation. *arXiv preprint arXiv:1907.10830*, 2019.

Diederik P Kingma and Jimmy Ba. Adam: A method for stochastic optimization. *arXiv preprint arXiv:1412.6980*, 2014.

Rolf Köhler, Christian Schuler, Bernhard Schölkopf, and Stefan Harmeling. Mask-specific inpainting with deep neural networks. In *German Conference on Pattern Recognition*, pp. 523–534. Springer, 2014.

Tuomas Kynkäänniemi, Tero Karras, Samuli Laine, Jaakko Lehtinen, and Timo Aila. Improved precision and recall metric for assessing generative models. In *Advances in Neural Information Processing Systems*, pp. 3929–3938, 2019.

Avisek Lahiri, Arnav Jain, Prabir Kumar Biswas, and Pabitra Mitra. Improving consistency and correctness of sequence inpainting using semantically guided generative adversarial network. *arXiv preprint arXiv:1711.06106*, 2017.

Avisek Lahiri, Arnav Kumar Jain, Sanskar Agrawal, Pabitra Mitra, and Prabir Kumar Biswas. Prior guided gan based semantic inpainting. In *Proceedings of the IEEE/CVF Conference on Computer Vision and Pattern Recognition*, pp. 13696–13705, 2020.

Jingyuan Li, Ning Wang, Lefei Zhang, Bo Du, and Dacheng Tao. Recurrent feature reasoning for image inpainting. In *Proceedings of the IEEE/CVF Conference on Computer Vision and Pattern Recognition*, pp. 7760–7768, 2020.

Guilin Liu, Fitsum A Reda, Kevin J Shih, Ting-Chun Wang, Andrew Tao, and Bryan Catanzaro. Image inpainting for irregular holes using partial convolutions. In *Proceedings of the European Conference on Computer Vision (ECCV)*, pp. 85–100, 2018.

Hongyu Liu, Bin Jiang, Yi Xiao, and Chao Yang. Coherent semantic attention for image inpainting. *arXiv preprint arXiv:1905.12384*, 2019a.

Hongyu Liu, Bin Jiang, Yibing Song, Wei Huang, and Chao Yang. Rethinking image inpainting via a mutual encoder-decoder with feature equalizations. *arXiv preprint arXiv:2007.06929*, 2020.

Ming-Yu Liu, Thomas Breuel, and Jan Kautz. Unsupervised image-to-image translation networks. In *Advances in neural information processing systems*, pp. 700–708, 2017.

Ming-Yu Liu, Xun Huang, Arun Mallya, Tero Karras, Timo Aila, Jaakko Lehtinen, and Jan Kautz. Few-shot unsupervised image-to-image translation. In *Proceedings of the IEEE International Conference on Computer Vision*, pp. 10551–10560, 2019b.

David Lopez-Paz and Maxime Oquab. Revisiting classifier two-sample tests. *arXiv preprint arXiv:1610.06545*, 2016.

Yuqing Ma, Xianglong Liu, Shihao Bai, Lei Wang, Aishan Liu, Dacheng Tao, and Edwin Hancock. Region-wise generative adversarial imageinpainting for large missing areas. *arXiv preprint arXiv:1909.12507*, 2019.

Qi Mao, Hsin-Ying Lee, Hung-Yu Tseng, Siwei Ma, and Ming-Hsuan Yang. Mode seeking generative adversarial networks for diverse image synthesis. In *Proceedings of the IEEE Conference on Computer Vision and Pattern Recognition*, pp. 1429–1437, 2019.

Lars Mescheder, Andreas Geiger, and Sebastian Nowozin. Which training methods for gans do actually converge? *arXiv preprint arXiv:1801.04406*, 2018.

Kamyar Nazeri, Eric Ng, Tony Joseph, Faisal Qureshi, and Mehran Ebrahimi. Edgeconnect: Generative image inpainting with adversarial edge learning. *arXiv preprint arXiv:1901.00212*, 2019.

Augustus Odena, Jacob Buckman, Catherine Olsson, Tom B Brown, Christopher Olah, Colin Raffel, and Ian Goodfellow. Is generator conditioning causally related to gan performance? *arXiv preprint arXiv:1802.08768*, 2018.

Taesung Park, Ming-Yu Liu, Ting-Chun Wang, and Jun-Yan Zhu. Semantic image synthesis with spatially-adaptive normalization. In *Proceedings of the IEEE Conference on Computer Vision and Pattern Recognition*, pp. 2337–2346, 2019.

Deepak Pathak, Philipp Krahenbuhl, Jeff Donahue, Trevor Darrell, and Alexei A Efros. Context encoders: Feature learning by inpainting. In *Proceedings of the IEEE conference on computer vision and pattern recognition*, pp. 2536–2544, 2016.

Pengda Qin, Weiran Xu, and William Yang Wang. Dsgan: Generative adversarial training for distant supervision relation extraction. *arXiv preprint arXiv:1805.09929*, 2018.

Jimmy SJ Ren, Li Xu, Qiong Yan, and Wenxiu Sun. Shepard convolutional neural networks. In *Advances in Neural Information Processing Systems*, pp. 901–909, 2015.

Yurui Ren, Xiaoming Yu, Ruonan Zhang, Thomas H Li, Shan Liu, and Ge Li. Structureflow: Image inpainting via structure-aware appearance flow. In *Proceedings of the IEEE International Conference on Computer Vision*, pp. 181–190, 2019.

Mark Sabini and Gili Rusak. Painting outside the box: Image outpainting with gans. *arXiv preprint arXiv:1808.08483*, 2018.

Min-cheol Sagong, Yong-goo Shin, Seung-wook Kim, Seung Park, and Sung-jea Ko. Pepsi: Fast image inpainting with parallel decoding network. In *Proceedings of the IEEE Conference on Computer Vision and Pattern Recognition*, pp. 11360–11368, 2019.

Mehdi SM Sajjadi, Olivier Bachem, Mario Lucic, Olivier Bousquet, and Sylvain Gelly. Assessing generative models via precision and recall. In *Advances in Neural Information Processing Systems*, pp. 5228–5237, 2018.

Tim Salimans and Durk P Kingma. Weight normalization: A simple reparameterization to accelerate training of deep neural networks. In *Advances in neural information processing systems*, pp. 901–909, 2016.

Tim Salimans, Ian Goodfellow, Wojciech Zaremba, Vicki Cheung, Alec Radford, and Xi Chen. Improved techniques for training gans. In *Advances in neural information processing systems*, pp. 2234–2242, 2016.

Jake Snell, Karl Ridgeway, Renjie Liao, Brett D Roads, Michael C Mozer, and Richard S Zemel. Learning to generate images with perceptual similarity metrics. In *2017 IEEE International Conference on Image Processing (ICIP)*, pp. 4277–4281. IEEE, 2017.

Yi Wang, Xin Tao, Xiaojuan Qi, Xiaoyong Shen, and Jiaya Jia. Image inpainting via generative multi-column convolutional neural networks. In *Advances in Neural Information Processing Systems*, pp. 331–340, 2018.

Yi Wang, Xin Tao, Xiaoyong Shen, and Jiaya Jia. Wide-context semantic image extrapolation. In *Proceedings of the IEEE Conference on Computer Vision and Pattern Recognition*, pp. 1399–1408, 2019a.

Ze Wang, Xiuyuan Cheng, Guillermo Sapiro, and Qiang Qiu. Stochastic conditional generative networks with basis decomposition. *arXiv preprint arXiv:1909.11286*, 2019b.

Sitao Xiang and Hao Li. On the effects of batch and weight normalization in generative adversarial networks. *arXiv preprint arXiv:1704.03971*, 2017.

Chaohao Xie, Shaohui Liu, Chao Li, Ming-Ming Cheng, Wangmeng Zuo, Xiao Liu, Shilei Wen, and Errui Ding. Image inpainting with learnable bidirectional attention maps. In *Proceedings of the IEEE International Conference on Computer Vision*, pp. 8858–8867, 2019.

Junyuan Xie, Linli Xu, and Enhong Chen. Image denoising and inpainting with deep neural networks. In *Advances in neural information processing systems*, pp. 341–349, 2012.

Wei Xiong, Jiahui Yu, Zhe Lin, Jimei Yang, Xin Lu, Connelly Barnes, and Jiebo Luo. Foreground-aware image inpainting. In *Proceedings of the IEEE conference on computer vision and pattern recognition*, pp. 5840–5848, 2019.

Zhaoyi Yan, Xiaoming Li, Mu Li, Wangmeng Zuo, and Shiguang Shan. Shift-net: Image inpainting via deep feature rearrangement. In *Proceedings of the European Conference on Computer Vision (ECCV)*, pp. 1–17, 2018.

Chao Yang, Xin Lu, Zhe Lin, Eli Shechtman, Oliver Wang, and Hao Li. High-resolution image inpainting using multi-scale neural patch synthesis. In *Proceedings of the IEEE Conference on Computer Vision and Pattern Recognition*, pp. 6721–6729, 2017.

Yang Yang, Xiaojie Guo, Jiayi Ma, Lin Ma, and Haibin Ling. Lafin: Generative landmark guided face inpainting. *arXiv preprint arXiv:1911.11394*, 2019a.

Zongxin Yang, Jian Dong, Ping Liu, Yi Yang, and Shuicheng Yan. Very long natural scenery image prediction by outpainting. In *Proceedings of the IEEE International Conference on Computer Vision*, pp. 10561–10570, 2019b.

Zili Yi, Hao Zhang, Ping Tan, and Minglun Gong. Dualgan: Unsupervised dual learning for image-to-image translation. In *Proceedings of the IEEE international conference on computer vision*, pp. 2849–2857, 2017.

Jiahui Yu, Zhe Lin, Jimei Yang, Xiaohui Shen, Xin Lu, and Thomas S Huang. Generative image inpainting with contextual attention. In *Proceedings of the IEEE Conference on Computer Vision and Pattern Recognition*, pp. 5505–5514, 2018.

Jiahui Yu, Zhe Lin, Jimei Yang, Xiaohui Shen, Xin Lu, and Thomas S Huang. Free-form image inpainting with gated convolution. In *Proceedings of the IEEE International Conference on Computer Vision*, pp. 4471–4480, 2019.

Tao Yu, Zongyu Guo, Xin Jin, Shilin Wu, Zhibo Chen, Weiping Li, Zhizheng Zhang, and Sen Liu. Region Normalization for Image Inpainting. *arXiv e-prints*, art. arXiv:1911.10375, Nov 2019.

Yanhong Zeng, Jianlong Fu, Hongyang Chao, and Baining Guo. Learning pyramid-context encoder network for high-quality image inpainting. In *Proceedings of the IEEE Conference on Computer Vision and Pattern Recognition*, pp. 1486–1494, 2019.

Lei Zhao, Qihang Mo, Sihuan Lin, Zhizhong Wang, Zhiwen Zuo, Haibo Chen, Wei Xing, and Dongming Lu. Uctgan: Diverse image inpainting based on unsupervised cross-space translation. In *Proceedings of the IEEE/CVF Conference on Computer Vision and Pattern Recognition*, pp. 5741–5750, 2020.

Chuanxia Zheng, Tat-Jen Cham, and Jianfei Cai. Pluralistic image completion. In *Proceedings of the IEEE Conference on Computer Vision and Pattern Recognition*, pp. 1438–1447, 2019.

Bolei Zhou, Agata Lapedriza, Aditya Khosla, Aude Oliva, and Antonio Torralba. Places: A 10 million image database for scene recognition. *IEEE transactions on pattern analysis and machine intelligence*, 40(6): 1452–1464, 2017.

Tong Zhou, Changxing Ding, Shaowen Lin, Xinchao Wang, and Dacheng Tao. Learning oracle attention for high-fidelity face completion. In *Proceedings of the IEEE/CVF Conference on Computer Vision and Pattern Recognition*, pp. 7680–7689, 2020.

Jun-Yan Zhu, Taesung Park, Phillip Isola, and Alexei A Efros. Unpaired image-to-image translation using cycle-consistent adversarial networks. In *Proceedings of the IEEE international conference on computer vision*, pp. 2223–2232, 2017a.

Jun-Yan Zhu, Richard Zhang, Deepak Pathak, Trevor Darrell, Alexei A Efros, Oliver Wang, and Eli Shechtman. Toward multimodal image-to-image translation. In *Advances in neural information processing systems*, pp. 465–476, 2017b.

APPENDIX A IMPLEMENTATION DETAILS

We mostly borrow the network details and hyperparameters from StyleGAN2 (Karras et al., 2019b), including the number of convolutional layers (2) at each level, the number of channels (64 at 512×512 resolution, doubled at each coarser level with a maximum of 512), architecture of the mapping network $\mathcal{M}$ (8-layer MLP), layer-wise noise injection, style mixing regularization (with a probability of 0.5 instead), non-saturating logistic loss (Goodfellow et al., 2014) with R_1 regularization (Mescheder et al., 2018) of $\gamma = 10$, and the Adam optimizer (Kingma & Ba, 2014) with a learning rate of 0.002.

Our conditional encoder $\mathcal{E}$ imitates a similar architecture as the discriminator but without the cross-level residual connections. Skip residual connections are used between each level of $\mathcal{E}$ and $\mathcal{D}$. To produce the conditional style representation, the final 4×4 feature map of $\mathcal{E}$ is flattened and passed through a fully connected layer of 1024 channels with a dropout rate of 0.5. The dropout layer keeps enabled during testing since we observe that it partially correlates to the inherent stochasticity.

Our model has 109M parameters in total. All the experiments are run on 8 cards of NVIDIA Tesla V100 GPUs. The batch size is 4 per GPU, 32 in total. The training length is 25M images unless specified, which takes about 1 week at 512×512 resolution.

APPENDIX B FREE-FORM MASK SAMPLING

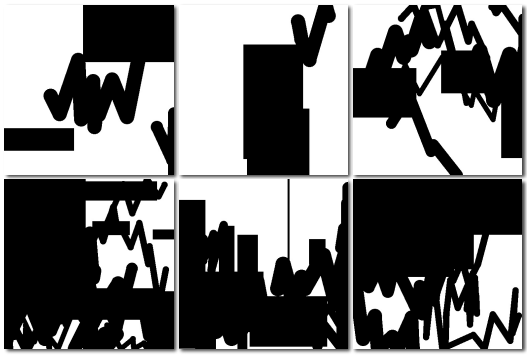

Figure 13: Random samples of free-form masks.

We sample free-form masks for training by simulating random brush strokes and rectangles. The algorithm of generating brush strokes is borrowed from DeepFillv2 (Yu et al., 2019), while the width of the brush is uniformly sampled within $[12, 48]$, the number of vertices is uniformly sampled within $[4, 18]$, and the number of strokes is uniformly sampled within $[0, 20]$. We then generate multiple rectangles with uniformly random widths, heights, and locations, while the number of up to full-size rectangles is uniformly sampled within $[0, 5]$ and the number of up to half-size rectangles is uniformly sampled within $[0, 10]$. See Fig. 13 for the sampled free-form masks. During evaluation, we use the same sampling strategy of free-form masks as used in training if no masked ratio is specified; otherwise, we repeatedly apply the same algorithm until the specified range is satisfied.

APPENDIX C USER STUDY

For the user study of image completion, we randomly sample the same number (256) of validation images, free-form masks (using the algorithm above), and the corresponding outputs from each method, for each dataset and each range of masked ratio. The user is given a pair of fake and the corresponding real images in each round and has 5 seconds to decide which one is fake or "don't know"; overtime rounds are also treated as "don't know". No user will see a real for more than once. To compute the user preference rate of fakes over reals, we regard a correct answer as 0, an incorrect answer as 1, and a "don't know" as 0.5. We have received totally 14336 rounds of answers from 28 participants. See Table 4 for the numerical results.

We adopt a similar protocol for the user study on COCO-Stuff. In each round, the user is given a pair of generated images of SPADE (Park et al., 2019) and ours using the same validation input. The user

Figure 14: Samples on Edges2Handbags.

Figure 15: Failure cases.

has 5 seconds to decide which one is preferred or "don't know"; overtime rounds are also treated as "don't know". We regard a "don't know" as 0.5. We have received 720 rounds of answers from 12 participants, among which 319 prefer ours, 189 prefer SPADE, and 212 "don't know".

APPENDIX D MORE QUANTITATIVE RESULTS

Table 5 presents the quantitative results for image completion across methods and masked ratios. Table 6 presents the quantitative results of the ablation experiment. Experiments demonstrate our superior performance at all masked ratios.

APPENDIX E MORE QUALITATIVE RESULTS

Fig. 14 presents our generated samples for image-to-image translation on the Edges2Handbags dataset under both $\psi = 1$ (which achieves superior fidelity) and $\psi = 3$ (which achieves superior diversity). See Fig. 16 for a qualitative comparison for image-to-image translation on the COCO-Stuff dataset. Extensive examples for free-form image completion are presented in Figs. 19-24.

APPENDIX F DISCUSSION

Large scale image completion is a challenging task that requires not only generative but also recognition capability. Although our model generates promising results in most of the cases, it sometimes fails to recognize the semantic information in the surrounding areas hence produces strange artifacts (see Fig. 15), especially in the challenging Places2 dataset that contains millions of scenes under various style and quality. The readers are encouraged to discover more examples from our interactive demo.

Table 4: User study results for image completion at different masked ratios among PatchMatch (Barnes et al., 2009), DeepFillv2 (retrained) (Yu et al., 2019), and ours.

Method	FFHQ					Places2				
	(0, .2)	(.2, .4)	(.4, .6)	(.6, .8)	(.8, 1)	(0, .2)	(.2, .4)	(.4, .6)	(.6, .8)	(.8, 1)
PatchMatch	10.7%	2.7%	3.2%	1.9%	2.1%	15.7%	4.1%	3.1%	1.7%	3.1%
DeepFillv2 (retrained)	40.6%	28.0%	17.9%	7.6%	2.7%	32.3%	19.1%	9.8%	3.4%	4.3%
Ours	**47.9%**	**44.8%**	**37.8%**	**36.0%**	**33.6%**	**40.3%**	**32.7%**	**18.7%**	**14.5%**	**13.8%**

Table 5: Quantitative comparison for image completion at different masked ratios among DeepFillv2 (official), DeepFillv2 (retrained) (Yu et al., 2019), and ours. Results are averaged over 5 runs.

Masked Ratio	Method	FFHQ			Places2		
		P-IDS (%)	U-IDS (%)	FID	P-IDS (%)	U-IDS (%)	FID
(0, .2)	DeepFillv2 (official)	6.4 ± 0.1	28.8 ± 0.2	1.78 ± 0.02	21.3 ± 0.2	42.6 ± 0.1	0.51 ± 0.01
	DeepFillv2 (retrained)	18.3 ± 0.3	40.3 ± 0.2	0.67 ± 0.00	21.2 ± 0.3	42.8 ± 0.1	0.47 ± 0.00
	Ours	$\mathbf{31.3 \pm 0.3}$	$\mathbf{44.4 \pm 0.3}$	$\mathbf{0.54 \pm 0.01}$	$\mathbf{33.3 \pm 0.2}$	$\mathbf{46.2 \pm 0.0}$	$\mathbf{0.33 \pm 0.00}$
(.2, .4)	DeepFillv2 (official)	0.0 ± 0.0	2.4 ± 0.1	16.30 ± 0.11	3.7 ± 0.1	24.5 ± 0.1	4.41 ± 0.03
	DeepFillv2 (retrained)	3.8 ± 0.2	22.0 ± 0.2	2.95 ± 0.03	5.1 ± 0.1	27.1 ± 0.1	3.50 ± 0.03
	Ours	$\mathbf{22.1 \pm 0.3}$	$\mathbf{37.5 \pm 0.2}$	$\mathbf{1.69 \pm 0.01}$	$\mathbf{20.6 \pm 0.3}$	$\mathbf{38.7 \pm 0.1}$	$\mathbf{1.74 \pm 0.02}$
(.4, .6)	DeepFillv2 (official)	0.0 ± 0.0	0.0 ± 0.0	46.11 ± 0.09	0.5 ± 0.0	10.7 ± 0.1	14.85 ± 0.06
	DeepFillv2 (retrained)	0.8 ± 0.0	11.1 ± 0.1	7.73 ± 0.09	1.4 ± 0.0	14.3 ± 0.1	11.16 ± 0.05
	Ours	$\mathbf{17.9 \pm 0.5}$	$\mathbf{32.1 \pm 0.2}$	$\mathbf{2.88 \pm 0.03}$	$\mathbf{14.6 \pm 0.2}$	$\mathbf{31.2 \pm 0.1}$	$\mathbf{4.77 \pm 0.03}$
(.6, .8)	DeepFillv2 (official)	0.0 ± 0.0	0.0 ± 0.0	96.58 ± 0.19	0.1 ± 0.0	3.1 ± 0.0	35.81 ± 0.14
	DeepFillv2 (retrained)	0.1 ± 0.0	3.2 ± 0.1	18.02 ± 0.33	0.5 ± 0.0	6.4 ± 0.0	25.75 ± 0.06
	Ours	$\mathbf{15.2 \pm 0.3}$	$\mathbf{27.9 \pm 0.2}$	$\mathbf{4.13 \pm 0.06}$	$\mathbf{11.5 \pm 0.1}$	$\mathbf{24.9 \pm 0.0}$	$\mathbf{9.64 \pm 0.04}$
(.8, 1)	DeepFillv2 (official)	0.0 ± 0.0	0.0 ± 0.0	179.12 ± 0.40	0.0 ± 0.0	0.0 ± 0.0	71.72 ± 0.16
	DeepFillv2 (retrained)	0.0 ± 0.0	0.0 ± 0.0	44.63 ± 0.75	0.1 ± 0.0	2.1 ± 0.0	51.52 ± 0.27
	Ours	$\mathbf{13.7 \pm 0.2}$	$\mathbf{24.1 \pm 0.2}$	$\mathbf{5.52 \pm 0.08}$	$\mathbf{9.8 \pm 0.1}$	$\mathbf{19.8 \pm 0.0}$	$\mathbf{15.27 \pm 0.06}$

Table 6: Ablation study among Vanilla, conditional modulation (C-Mod), and our co-modulation (Co-Mod), as illustrated in Figs. 2(b) to 2(d), for image completion on the FFHQ dataset. Vanilla completely fails; our co-modulation dominates the conditional modulated version at all masked ratios and especially when the masked ratio becomes large. Results are averaged over 5 runs.

Masked Ratio	Method	P-IDS (%)	U-IDS (%)	FID
(0.0, 0.2)	Vanilla	0.6 ± 0.1	3.0 ± 0.1	71.72 ± 0.65
	C-Mod	30.7 ± 0.3	44.3 ± 0.2	0.55 ± 0.01
	Co-Mod	$\mathbf{31.3 \pm 0.3}$	$\mathbf{44.4 \pm 0.3}$	$\mathbf{0.54 \pm 0.01}$
(0.2, 0.4)	Vanilla	0.0 ± 0.0	0.0 ± 0.0	152.79 ± 0.37
	C-Mod	21.1 ± 0.2	36.9 ± 0.2	1.78 ± 0.02
	Co-Mod	$\mathbf{22.1 \pm 0.3}$	$\mathbf{37.5 \pm 0.2}$	$\mathbf{1.69 \pm 0.01}$
(0.4, 0.6)	Vanilla	0.0 ± 0.0	0.0 ± 0.0	192.24 ± 0.44
	C-Mod	16.3 ± 0.3	30.9 ± 0.3	3.03 ± 0.02
	Co-Mod	$\mathbf{17.9 \pm 0.5}$	$\mathbf{32.1 \pm 0.2}$	$\mathbf{2.88 \pm 0.03}$
(0.6, 0.8)	Vanilla	0.0 ± 0.0	0.0 ± 0.0	247.68 ± 1.28
	C-Mod	13.6 ± 0.2	26.2 ± 0.1	4.42 ± 0.02
	Co-Mod	$\mathbf{15.2 \pm 0.3}$	$\mathbf{27.9 \pm 0.2}$	$\mathbf{4.13 \pm 0.06}$
(0.8, 1.0)	Vanilla	0.0 ± 0.0	0.0 ± 0.0	286.53 ± 0.93
	C-Mod	11.9 ± 0.1	22.2 ± 0.1	5.96 ± 0.03
	Co-Mod	$\mathbf{13.7 \pm 0.2}$	$\mathbf{24.1 \pm 0.2}$	$\mathbf{5.52 \pm 0.08}$

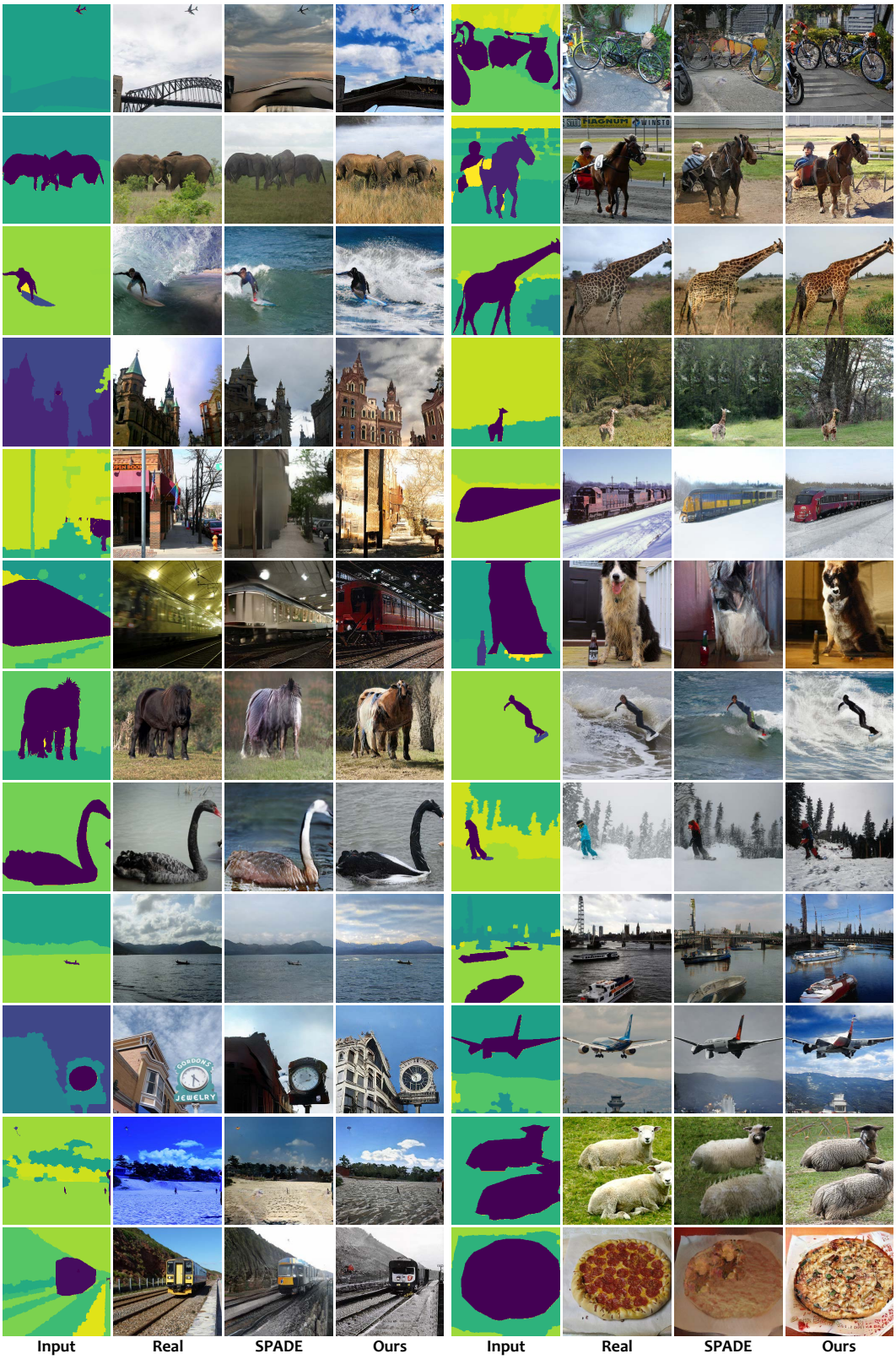

Figure 16: Qualitative comparison between SPADE (Park et al., 2019) and ours for image-to-image translation on the COCO-Stuff validation set (Caesar et al., 2018) (labels to photos).

Figure 17: Our image completion results w.r.t. different masks. Our method successfully bridges differently conditioned situations, from small-scale inpainting to large-scale completion (left to right). The original images are sampled at 512×512 resolution from the FFHQ dataset (Karras et al., 2019a) within a 10k validation split.

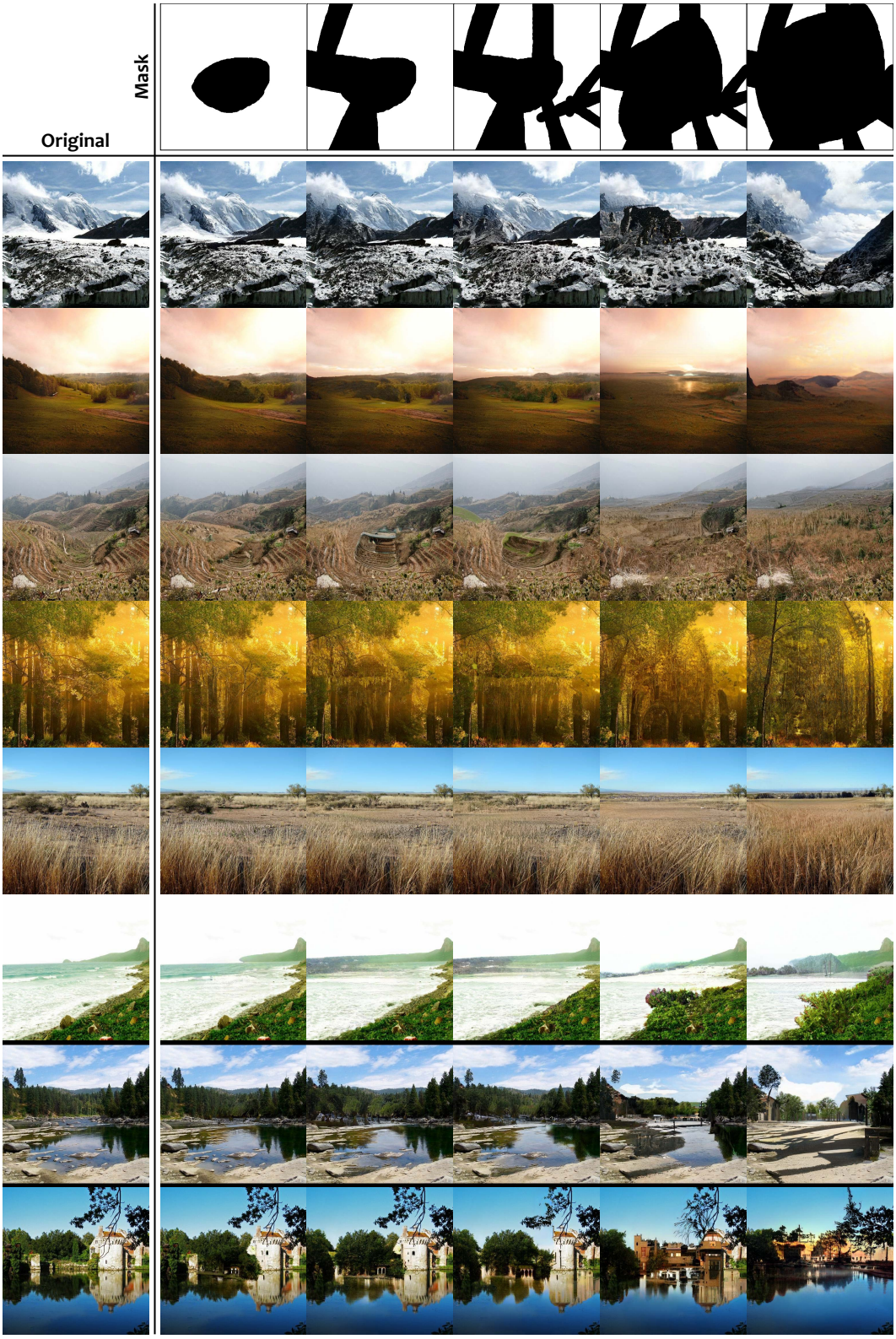

Figure 18: Our image completion results w.r.t. different masks. Our method successfully bridges differently conditioned situations, from small-scale inpainting to large-scale completion (left to right). The original images are sampled at 512×512 resolution from the Places2 validation set (Zhou et al., 2017).

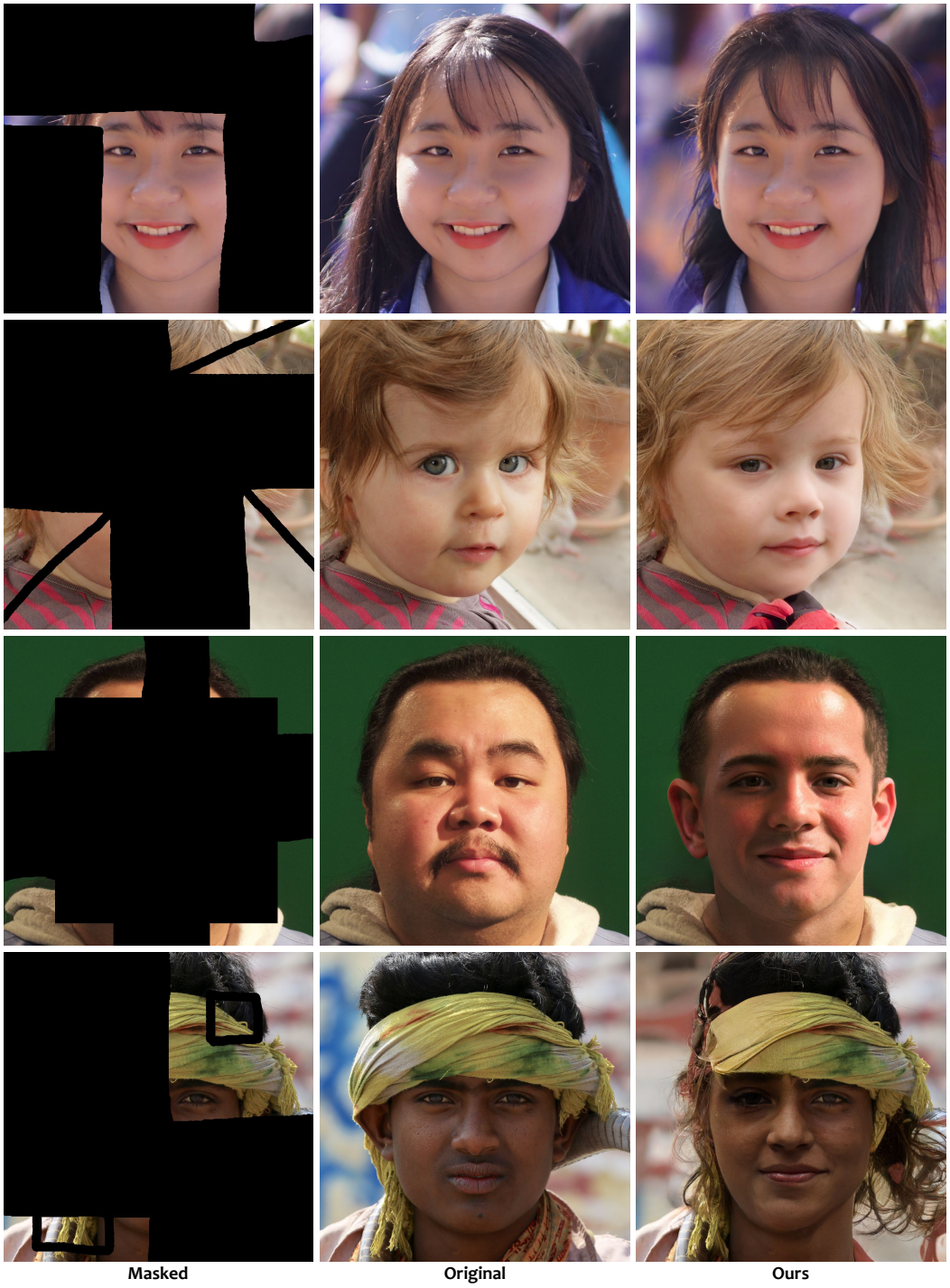

Figure 19: Qualitative examples for image completion at 1024×1024 resolution. The original images are sampled from the FFHQ dataset (Karras et al., 2019a) within a 10k validation split.

Figure 20: Qualitative examples for image completion at 1024×1024 resolution. The original images are sampled from the FFHQ dataset (Karras et al., 2019a) within a 10k validation split.

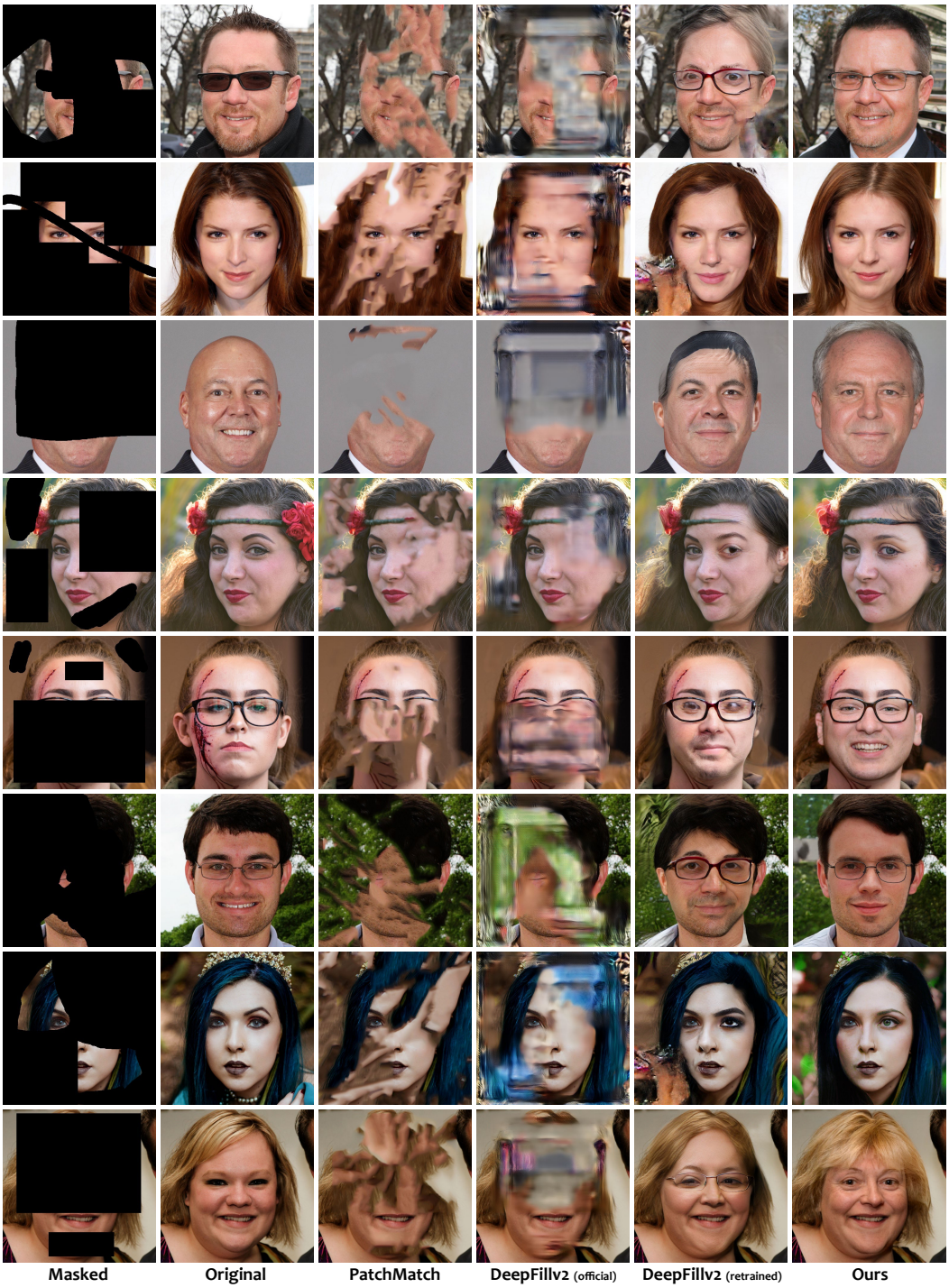

Figure 21: Qualitative examples for image completion among PatchMatch (Barnes et al., 2009), DeepFillv2 (Yu et al., 2019), and ours. The original images are sampled at 512×512 resolution from the FFHQ dataset (Karras et al., 2019a) within a 10k validation split.

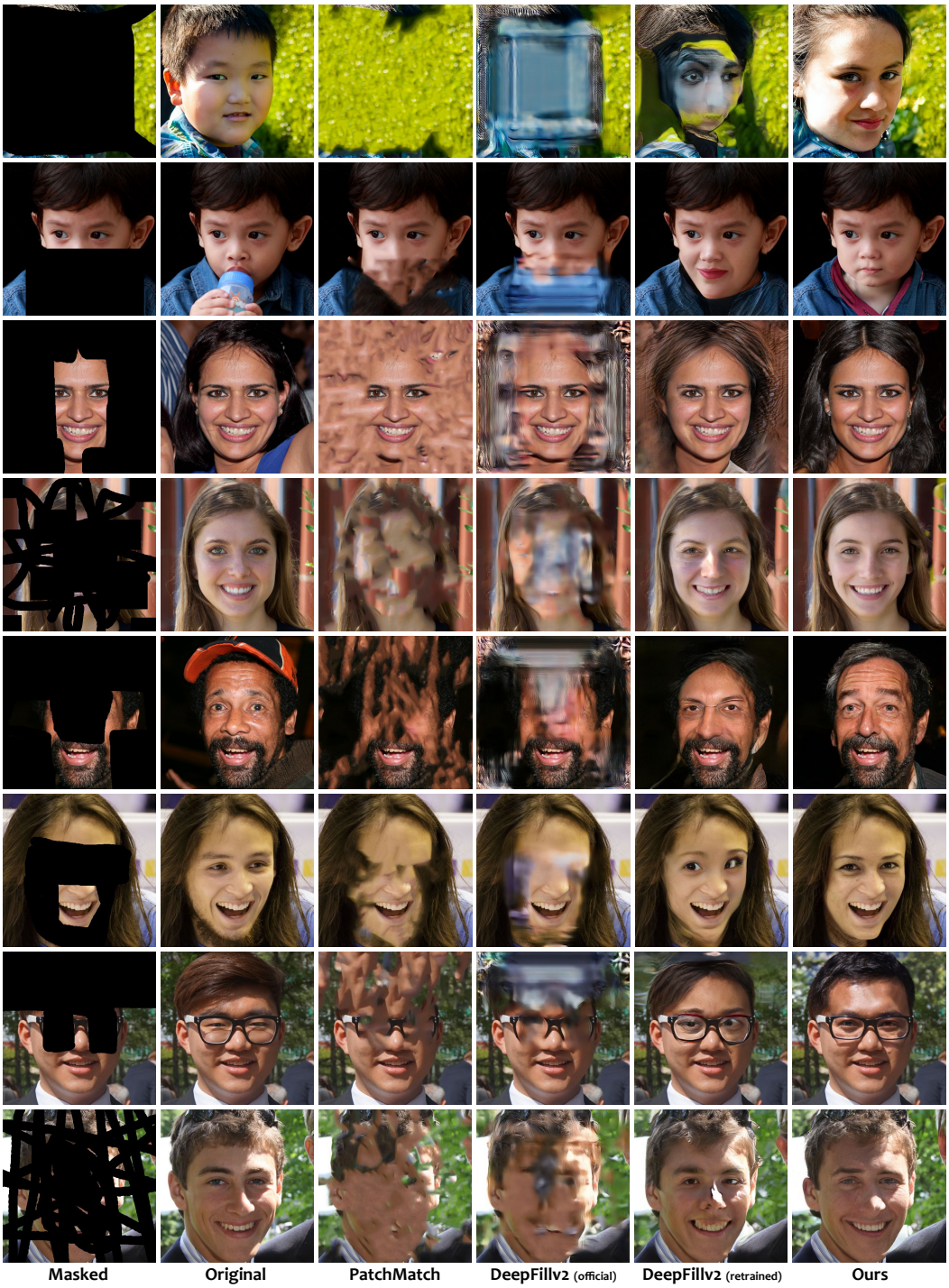

Figure 22: Qualitative examples for image completion among PatchMatch (Barnes et al., 2009), DeepFillv2 (Yu et al., 2019), and ours. The original images are sampled at 512×512 resolution from the FFHQ dataset (Karras et al., 2019a) within a 10k validation split.

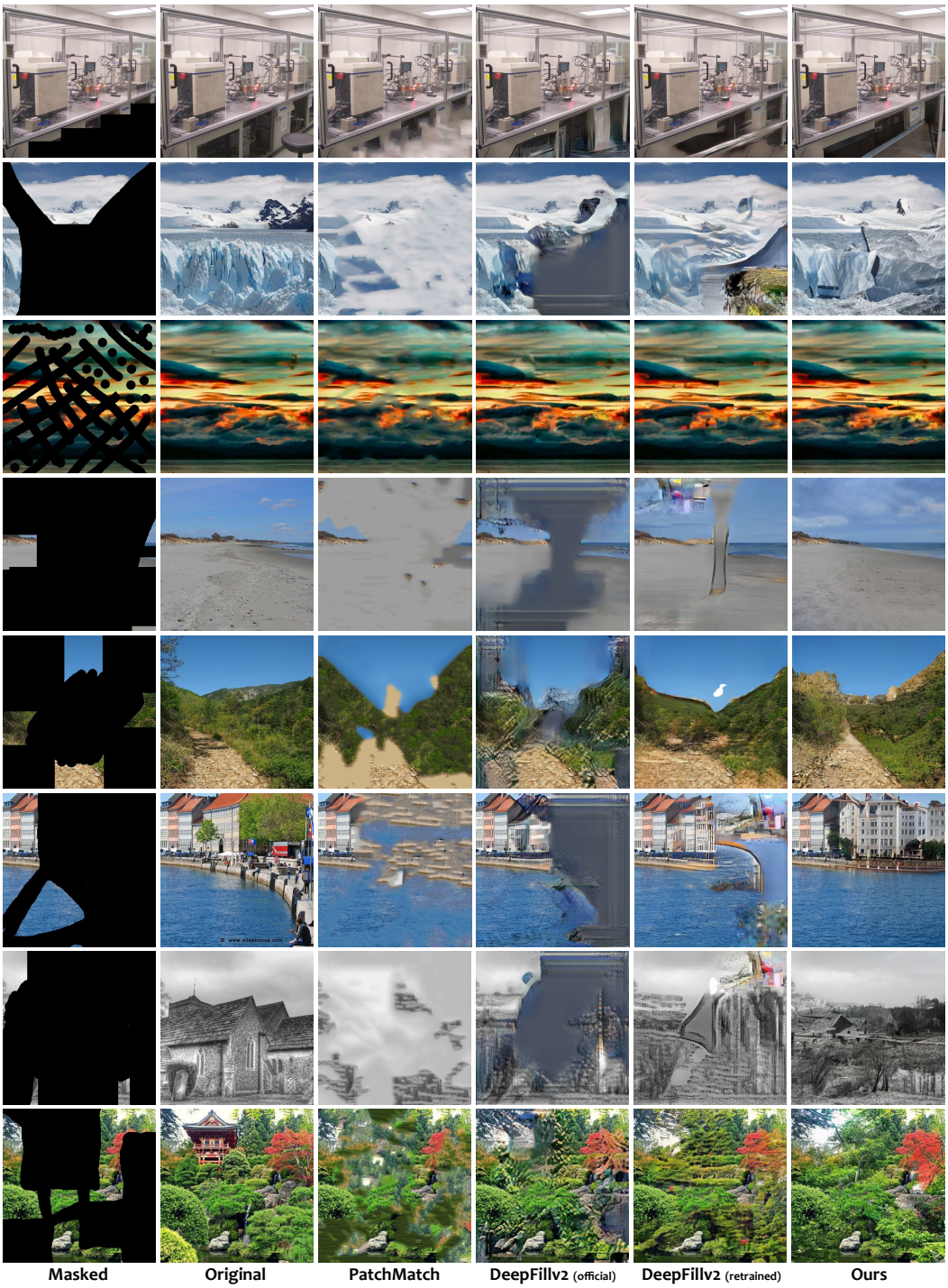

Figure 23: Qualitative examples for image completion among PatchMatch (Barnes et al., 2009), DeepFillv2 (Yu et al., 2019), and ours. The original images are sampled at 512×512 resolution from the Places2 validation set (Zhou et al., 2017).

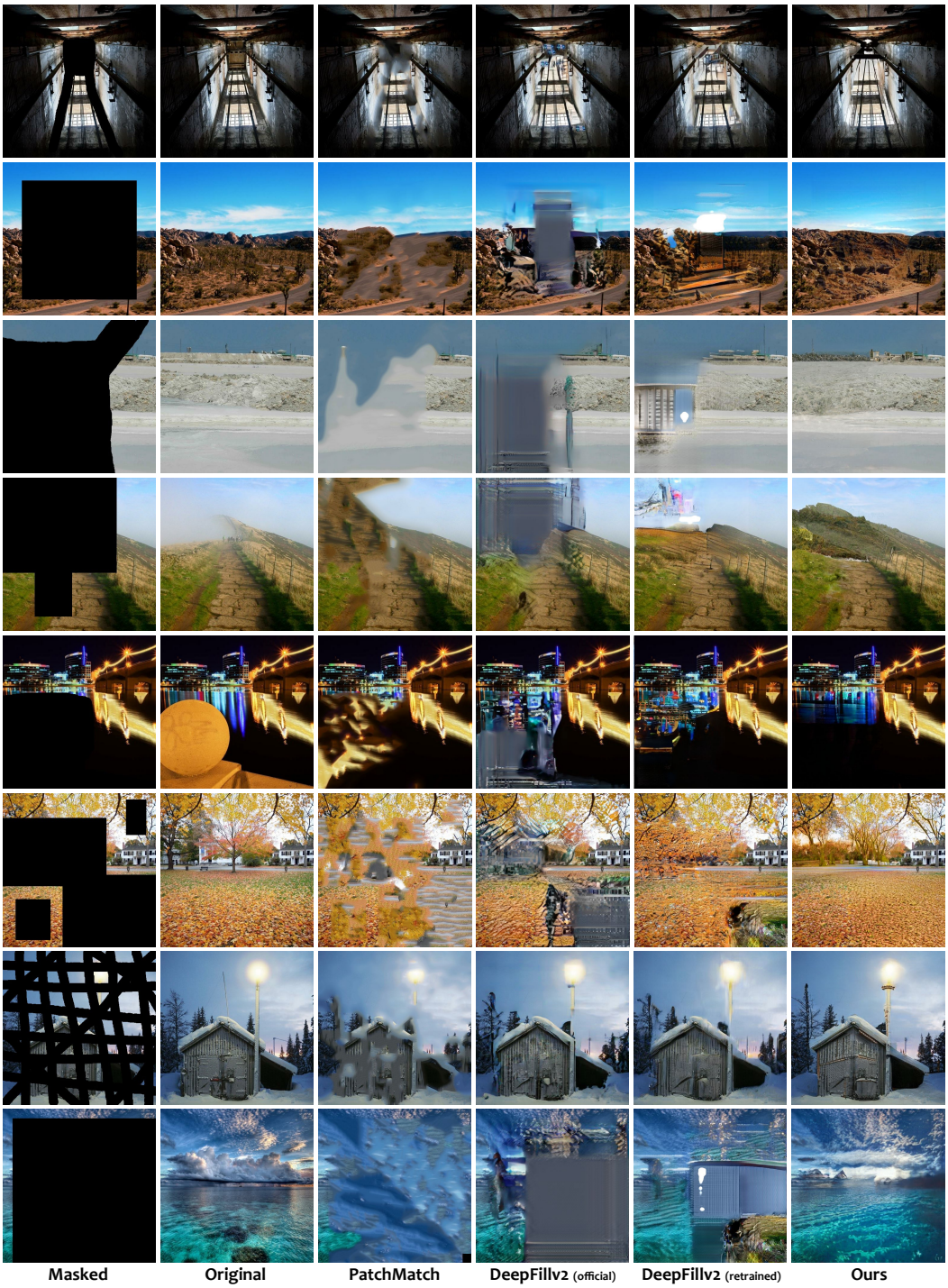

Figure 24: Qualitative examples for image completion among PatchMatch (Barnes et al., 2009), DeepFillv2 (Yu et al., 2019), and ours. The original images are sampled at 512×512 resolution from the Places2 validation set (Zhou et al., 2017).